

Parallax QAMA: Novel Downlink Multiple Access for MISO Systems with Simple Receivers

Jie Huang, Ming Zhao, *Member, IEEE*, Shengli Zhou, *Fellow, IEEE*, Ling Qiu, *Member, IEEE*, Jinkang Zhu, *Life Member, IEEE*,

Abstract—In this paper, we propose a novel downlink multiple access system with a multi-antenna transmitter and two single-antenna receivers, inspired by the underlying principles of hierarchical quadrature amplitude modulation (H-QAM) based multiple access (QAMA) and space-division multiple access (SDMA). In the proposed scheme, coded bits from two users are split and assigned to one shared symbol and two private symbols carried by different beams. Based on joint symbol mapping of H-QAM constellations and phase-aligned precoding at the transmitter, each receiver observes a different H-QAM constellation with Gray mapping, a unique parallax feature not shared by existing schemes. In addition to avoiding successive interference cancellation (SIC), each user independently demodulates its own bits on separate I and Q branches with calculations based on closed-form expressions. Hence the receiver complexity is on par with that of orthogonal multiple access (OMA), which is much lower than that in other competing alternatives such as non-orthogonal multiple access (NOMA) and rate-splitting multiple access (RSMA). We carry out system optimization and determine the achievable rate region. Numerical results show that the proposed system has a larger rate region relative to other benchmark schemes with receivers not using SIC, and even achieves a comparable rate region to those benchmark schemes with SIC receivers.

Index Terms—Multiple access, MISO, hierarchical QAM, SIC-free.

I. INTRODUCTION

With the increasing demand for massive connectivity and high spectrum efficiency (SE), next-generation multiple access (NGMA) has garnered significant attention from researchers [1]. In particular, the downlink multiple access design has evolved from conventional orthogonal multiple access (OMA) schemes, which leverage orthogonality in frequency, time and code domains, to embrace more efficient and flexible strategies. For the single-input single-output (SISO) broadcast channel (BC), it has been proven that the combination of superposition coding (SC) and successive interference cancellation (SIC) achieves the capacity region [2], [3]. In the case of the multiple-input single-output (MISO) Gaussian BC,

dirty paper coding (DPC) has been shown to be the capacity-achieving strategy [4]. However, DPC suffers from the high complexity of the nonlinear processing at the transmitter, which poses challenges to its practical implementations.

In contrast to DPC, space-division multiple access (SDMA) based on linear precoding has been widely adopted in multi-antenna systems owing to its lower transmitter complexity and near-capacity performance, particularly when user channels are nearly orthogonal with similar channel strengths [5], [6]. In SDMA systems, inter-user interference is suppressed or even eliminated by skillful precoding, which enables low receiver complexity. However, the performance of SDMA decreases quickly in overloaded scenarios where user channels are highly correlated [7].

Inspired by the capacity-achieving performance in single-antenna systems, non-orthogonal multiple access (NOMA) relying on SC at the transmitter and SIC at the receiver is extended to the multi-antenna setup [8]. Existing literature shows that multi-antenna NOMA achieves significant performance gains over OMA systems in an overloaded system that serves users with highly correlated channels and diverse channel strengths [9], [10].

Over the past decade, a noticeable advancement in the area of multi-antenna multiple access has been the emergence of rate-splitting multiple access (RSMA) [11]. It unifies SDMA, NOMA and OMA into one general framework [12]. In conventional downlink RSMA systems, the transmitter splits and encodes all users' messages into a common stream and several private streams, which are then superposed and transmitted based on linear precoding. SIC-based receivers are utilized to decode and remove the common stream from the received signal before decoding the intended private stream. By partially treating interference as noise and partially decoding interference, RSMA shows numerous advantages, e.g. the achievable rate region close to that of DPC [13], the robustness to imperfect channel state information at transmitter (CSIT) [14], [15], significant improvements in terms of spectral efficiency [16], energy efficiency [17] and degree of freedom (DoF) [18]. Furthermore, the advantages of RSMA are experimentally demonstrated on a software-defined radio testbed [19].

The research on NOMA and RSMA generally relies on SIC to decode and eliminate interference caused by message superposition. On the one hand, SIC increases the computational complexity of the receiver, especially as the number of SIC layers grows in multi-user scenarios [20]. On the other hand, it is difficult to implement perfect SIC in a practical system. In particular, error propagation due to imperfect SIC

The work of J. Huang, M. Zhao and J. Zhu was supported by the National Key R&D Program of China under Grant 2022YFB2902005.

Jie Huang, Ming Zhao, and Ling Qiu are with CAS Key Laboratory of Wireless-Optical Communications, University of Science and Technology of China (USTC), Hefei, Anhui Province, 230027, P. R. China (e-mail: ziven@mail.ustc.edu.cn, zhaoming@ustc.edu.cn, lqiu@ustc.edu.cn).

Shengli Zhou is with Department of Electrical and Computer Engineering, University of Connecticut, 371 Fairfield Way, Unit 4157, Storrs, CT 06269-4157 (e-mail: shengli.zhou@uconn.edu).

Jinkang Zhu is with Dept. of Electronic Engineering and Information Science, University of Science and Technology of China (USTC), Hefei, Anhui Province, 230027, P. R. China (e-mail: jkzhu@ustc.edu.cn).

can significantly undermine system performance [21]. The limitations of SIC underscore the need to explore SIC-free multiple access schemes.

A. Downlink Multiple Access with SIC-free Receivers

In a downlink system with a single-antenna transmitter, SIC-free transmission schemes based on discrete constellations and lattice partitioning have been proposed in [22] and [23], allowing single-user decoding and achieving rates within a constant gap from the capacity region. In [24], the receiver employing modulo operation instead of SIC is used in a multi-user scheduling setting. The complexity reduction however comes with the cost of performance. A hierarchical quadrature amplitude modulation (H-QAM) based multiple access scheme, termed QAMA, has been proposed in [25], which assigns users separate bit streams from a tunable hierarchical constellation. Even using simpler receiver processing, QAMA achieves a similar rate region to multi-user superposition transmission (MUST) in the 3GPP standard for 5G cellular systems with SIC receivers [26]. In [27], a single-antenna system design based on rate splitting makes an effort to eliminate SIC where the common and private streams are carried in the in-phase and quadrature components of the transmitted signal.

In the systems with a multiple-antenna transmitter, there have been recent works with SIC-free receivers. Taking advantage of the additional degrees of freedom (DoF) offered by the polarization domain, a dual-polarized massive multiple-input multiple-output (MIMO) RSMA system with three transmission strategies is proposed in [28] to address practical issues caused by imperfect SIC. In particular, the first strategy avoids the use of SIC at the receiver. Practical non-SIC receivers are considered in the 1-Layer RSMA system to assess the performance of RSMA without SIC-based receivers [29], [30]. In these works, the superiority of RSMA over SDMA remains to some extent even without SIC at receivers. Numerical results also confirm performance gaps in terms of rate region between RSMA systems with SIC receivers and non-SIC receivers.

B. Contributions

In this paper, we propose a novel downlink multiple access scheme, termed parallax QAMA (PxQAMA), where a multi-antenna transmitter simultaneously serves two single-antenna users. In each channel use, coded bits from two users are split and mapped into one shared symbol and two private symbols, which are drawn from individual H-QAM constellations with different sizes and distance parameters. Specifically, bit streams from the shared symbol are assigned to two users as in the QAMA framework, while each private symbol carries bit streams intended for a single user. Carried on separate beams, the three symbols are superimposed and transmitted together. The innovative designs of the proposed system are two-fold:

- The shared and private symbols are jointly Gray-mapped to ensure that the composite constellation remains Gray-coded.

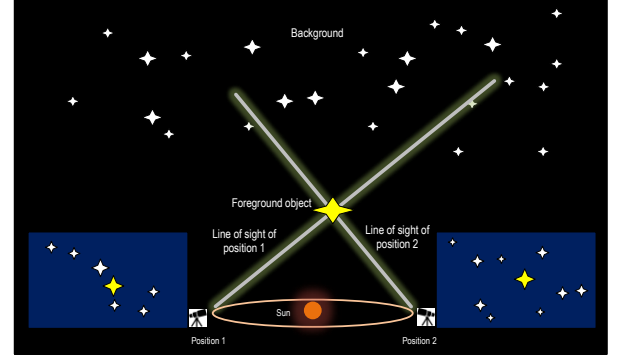


Fig. 1. Stellar parallax refers to the apparent shift in a star's position relative to the background as observed from the Earth, resulting in a composite pattern that varies with the Earth's motion. Similarly, an individual composite constellation is observed by each user due to different channels and precoding vectors in PxQAMA systems.

- The orthogonality constraint and phase alignment constraint are imposed on the precoding design.

At the receiver side, each user observes a Gray-coded H-QAM constellation, which appears similar to QAMA though it is actually formed by the over-the-air superposition of the shared and private symbols. Moreover, the received constellations differ across users, as they have user-specific distance parameters shaped by their channels, resembling stellar parallax and inspiring the name, as shown in Fig. 1¹. Note that the parallax effect is not available in either QAMA or SDMA, where each user sees the same constellation as designed by the transmitter. This parallax effect is also not applicable to RSMA systems, where the receiver does not see a regular constellation.

The contributions of this paper are summarized as follows.

- The PxQAMA framework ensures low-complexity receiver processing. Each user only decodes the assigned bit streams in the shared symbol and the intended private symbol without consideration of other users. Not only does it avoid the use of SIC, but it also enables soft demapping based on closed-form expressions on the I and Q branches independently, thanks to the Gray mapping. The receiver of PxQAMA remains as simple as in an OMA system, which is lower than other competing alternatives, including the SIC-free receivers presented for RSMA in [30].
- The PxQAMA system is optimized, with closed-form expressions on the precoder directions and phases. The optimization framework is presented to determine the achievable rate region.
- Comparing the proposed system against mainstream multiple-access benchmarks, simulation results demonstrate that PxQAMA achieves superior performance with the simplest receiver. Unlike SDMA and NOMA, whose advantages are typically confined to specific channel conditions, PxQAMA performs consistently well in various scenarios. Compared to RSMA with SIC-free receivers, PxQAMA achieves a larger rate region with a simpler receiver. Even compared to the RSMA with SIC-based

¹The picture is adapted from <https://www.space.com/30417-parallax.html>

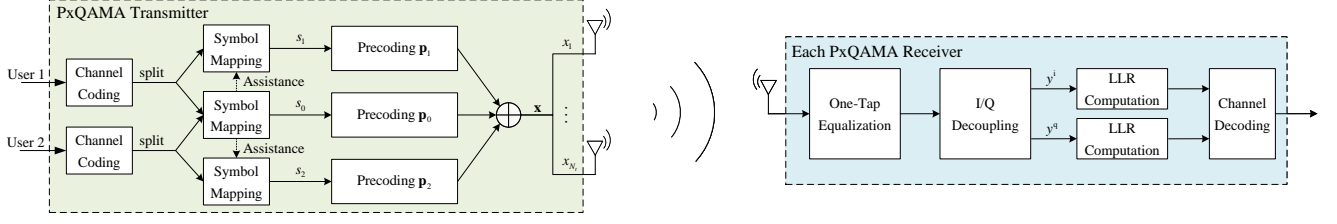


Fig. 2. The transmitter and receiver diagram for the two-user PxQAMA system.

receivers, PxQAMA achieves a comparable rate region in most cases.

While the focus of this paper is on a two-user system, the extension to multiple users is outlined, and an example of practical design with finite transmission modes is provided. Thanks to the receiver simplicity and outstanding performance, PxQAMA is a promising downlink multiple access scheme for future wireless networks, especially when the receiver complexity is the main bottleneck for real time signal processing or on low-cost computation devices.

The rest of the paper is organized as follows. The system model and the transceiver designs are presented in Section II. System optimization and the achievable rate region for the system are developed in Section III. The achieved rate regions are compared in Section IV and conclusions are collected in Section V.

Notation: Vectors and matrices are denoted by lower case and upper case of bold letters; the conjugate transpose of vector \mathbf{v} is denoted by \mathbf{v}^H ; $\Re\{\cdot\}$ and $\Im\{\cdot\}$ indicate the real and imaginary part of a complex number; $\|\cdot\|$ is the Euclidean norm; $\mathbb{E}[\cdot]$ refers to the statistic expectation.

II. SYSTEM DESCRIPTION

We consider a downlink system where a transmitter with N_t antennas serves $N_u = 2$ single-antenna users. Denoting the channel vector between the transmitter and user u as $\mathbf{h}_u \in \mathbb{C}^{N_t \times 1}$, the received signal at user u is

$$y_u = \mathbf{h}_u^H \mathbf{x} + w_u, \quad u \in \{1, 2\}, \quad (1)$$

where \mathbf{x} is the transmitted signal vector and w_u is the additive white Gaussian noise (AWGN) at user u that follows circularly symmetric complex Gaussian distribution with zero mean and variance σ^2 .

Fig. 2 depicts the proposed system diagram. As in an OMA system, each user has a separate channel encoder and channel decoder, and the novel system component is on the modulator for downlink multiple access. As shown in Fig. 2, the coded bits from two users are split and mapped into one shared symbol s_0 and two private symbols s_1, s_2 . The shared symbol carries bit streams assigned to both users, as in the QAMA framework, while each private symbol carries bit streams intended for a single user. At each channel use, the transmitted signal vector \mathbf{x} is

$$\mathbf{x} = \mathbf{p}_0 s_0 + \mathbf{p}_1 s_1 + \mathbf{p}_2 s_2, \quad (2)$$

where $\mathbf{p}_i \in \mathbb{C}^{N_t \times 1}$, $i \in \{0, 1, 2\}$, is the precoding vector corresponding to s_i .

The constellations for s_0, s_1 and s_2 are drawn from hierarchical M -ary QAM (H-MQAM) constellations with different sizes and distance parameters. For symbol s_i , the H-QAM constellation can be decomposed into a 2^{m_i} -PAM on the I branch and a 2^{n_i} -PAM on the Q branch, and hence carries $m_i + n_i$ bits per symbol [31], [32]. Define the collection of all the bits corresponding to symbol s_i as:

$$\mathcal{S}_i := \{b_{i,\kappa}^i\}_{\kappa=1}^{m_i} \cup \{b_{i,l}^q\}_{l=1}^{n_i}, \quad (3)$$

and the collection of the distance parameters as:

$$\mathcal{D}_i := \{d_{i,\kappa}^i\}_{\kappa=1}^{m_i} \cup \{d_{i,l}^q\}_{l=1}^{n_i}. \quad (4)$$

Each constellation is normalized to have unit energy that requires:

$$\sum_{\kappa=1}^{m_i} (d_{i,\kappa}^i)^2 + \sum_{l=1}^{n_i} (d_{i,l}^q)^2 = 1. \quad (5)$$

On each branch, the distance parameter corresponding to the lower-layer bit should be at least twice that of the higher-layer bit, i.e. $d_{i,\kappa}^i \geq 2d_{i,\kappa+1}^i$, $d_{i,l}^q \geq 2d_{i,l+1}^q$, to preserve the correct ordering of the constellation.

With perfect channel state information (CSI) at the transmitter, the system aims to optimize the data rates for both users while maintaining simple processing at each receiver. We next present the framework for the transmitter and receiver, while deferring the system optimization to Section III.

A. Transmitter Design

The PxQAMA framework judiciously designs the symbol mappers and the precoders at the transmitter.

1) *Joint Symbol Mapping:* The shared symbol s_0 adopts conventional Gray mapping for H-QAM [31], [32]. As clarified in Appendix A, the information symbol in Gray mapping is related to the information bits as

$$\begin{cases} \Re\{s_0\} = \sum_{\kappa=1}^{m_0} (-1)^{(1+\sum_{j=1}^{\kappa} b_{0,j}^i)} d_{0,\kappa}^i \\ \Im\{s_0\} = \sum_{l=1}^{n_0} (-1)^{(1+\sum_{j=1}^l b_{0,j}^q)} d_{0,l}^q. \end{cases} \quad (6)$$

For private symbols s_1 and s_2 , we propose a novel mapping rule as

$$\begin{cases} \Re\{s_i\} = (-1)^{(1+\sum_{\kappa=1}^{m_0} b_{0,\kappa}^i)} \sum_{\kappa=1}^{m_i} (-1)^{(\sum_{j=1}^{\kappa} b_{i,j}^i)} d_{i,\kappa}^i, \\ \Im\{s_i\} = (-1)^{(1+\sum_{l=1}^{n_0} b_{0,l}^q)} \sum_{l=1}^{n_i} (-1)^{(\sum_{j=1}^l b_{i,j}^q)} d_{i,l}^q. \end{cases} \quad (7)$$

Apparently, the Gray mapping for s_1, s_2 is dependent on the bits in s_0 . This mapping rule allows the following effects.

- $s_0 + c_1 s_1$ has Gray mapping for the collection of bits in \mathcal{S}_0 and \mathcal{S}_1 , where c_1 is a suitable positive constant.
- $s_0 + c_2 s_2$ has Gray mapping for the collection of bits in \mathcal{S}_0 and \mathcal{S}_2 where c_2 is a suitable positive constant.

An illustration of this effect is provided in Appendix A.

2) *Constraints on Precoding Vectors*: We adopt the following constraints on the precoding vectors.

- Direction control for \mathbf{p}_1 and \mathbf{p}_2 :

$$\mathbf{h}_1^H \mathbf{p}_2 = 0, \quad \mathbf{h}_2^H \mathbf{p}_1 = 0. \quad (8)$$

- Phase alignment for \mathbf{p}_1 and \mathbf{p}_2 :

$$\begin{cases} e^{j\angle(\mathbf{h}_1^H \mathbf{p}_1)} = e^{j\angle(\mathbf{h}_1^H \mathbf{p}_0)} = e^{j\Phi_1}, \\ e^{j\angle(\mathbf{h}_2^H \mathbf{p}_2)} = e^{j\angle(\mathbf{h}_2^H \mathbf{p}_0)} = e^{j\Phi_2}, \end{cases} \quad (9)$$

where $\angle(\cdot)$ is the phase of a complex number.

The direction and phase of \mathbf{p}_0 are left for optimization.

B. The Parallax Effect

Subject to the direction control in (8), the received signal for user u , $u = 1, 2$, can be expressed as

$$y_u = \mathbf{h}_u^H \mathbf{p}_0 s_0 + \mathbf{h}_u^H \mathbf{p}_u s_u + w_u. \quad (10)$$

For brevity, define the following variables:

$$G_u = \sqrt{|\mathbf{h}_u^H \mathbf{p}_0|^2 + |\mathbf{h}_u^H \mathbf{p}_u|^2}, \quad (11)$$

$$\beta_{u,0} = \frac{|\mathbf{h}_u^H \mathbf{p}_0|}{G_u}, \quad \beta_{u,u} = \frac{|\mathbf{h}_u^H \mathbf{p}_u|}{G_u}. \quad (12)$$

With the phases aligned in (9), one can simplify (10) as

$$y_u = e^{j\Phi_u} G_u (\beta_{u,0} s_0 + \beta_{u,u} s_u) + w_u. \quad (13)$$

Now introduce a composite symbol formed by s_0 and s_u as:

$$\tilde{s}_u = \beta_{u,0} s_0 + \beta_{u,u} s_u. \quad (14)$$

The input-output relationship in (13) is equivalent to

$$y_u = e^{j\Phi_u} G_u \tilde{s}_u + w_u. \quad (15)$$

Let us inspect the symbol \tilde{s}_u . It can be viewed as a symbol drawn from a H-QAM constellation with $m_0 + m_u$ bits on the I-branch and $n_0 + n_u$ bits on the Q-branch. Indeed, let us define the equivalent bits and distances as

$$\tilde{b}_{u,\kappa}^i = \begin{cases} b_{0,\kappa}^i, & \text{if } \kappa \leq m_0 \\ b_{u,\kappa-m_0}^i, & \text{if } \kappa > m_0 \end{cases} \quad (16)$$

$$\tilde{b}_{u,l}^q = \begin{cases} b_{0,l}^q, & \text{if } l \leq n_0 \\ b_{u,l-n_0}^q, & \text{if } l > n_0 \end{cases} \quad (17)$$

$$\tilde{d}_{u,\kappa}^i = \begin{cases} \beta_{u,0} d_{0,\kappa}^i, & \text{if } \kappa \leq m_0 \\ \beta_{u,u} d_{u,\kappa-m_0}^i, & \text{if } \kappa > m_0 \end{cases} \quad (18)$$

$$\tilde{d}_{u,l}^q = \begin{cases} \beta_{u,0} d_{0,l}^q, & \text{if } l \leq n_0 \\ \beta_{u,u} d_{u,l-n_0}^q, & \text{if } l > n_0. \end{cases} \quad (19)$$

By expressing \tilde{s}_u as:

$$\begin{cases} \Re\{\tilde{s}_u\} = \sum_{\kappa=1}^{m_0+m_u} (-1)^{(1+\sum_{j=1}^{\kappa} \tilde{b}_{u,j}^i)} \tilde{d}_{u,\kappa}^i, \\ \Im\{\tilde{s}_u\} = \sum_{l=1}^{n_0+n_u} (-1)^{(1+\sum_{j=1}^l \tilde{b}_{u,j}^q)} \tilde{d}_{u,l}^q, \end{cases} \quad (20)$$

one can see that Gray mapping from bits to symbols is maintained. Also, the constellation for \tilde{s}_u has unit energy as the distances in (18) and (19) satisfy the constraint in (5).

We emphasize that the equivalent constellations for user 1 and user 2 are different as they have different distance parameters shaped by their channels. Inspired by the terminology from astronomy (Fig. 1), we refer to this as the parallax effect of the proposed system design. Note that this parallel effect is absent in QAMA and SDMA systems, where each user sees the same constellation as designed by the transmitter. This parallax effect is also not applicable to RSMA systems, where the receiver does not see a regular constellation.

Fig. 3 provides an illustration with s_0, s_1, s_2 drawn from QPSK constellations, while each receiver observes a different H-16QAM.

Remark: A similar layered constellation structure could be observed at the receiver of layered division multiplexing (LDM) systems in Advanced Television Systems Committee (ATSC) 3.0 standard [33], where the core and extended layers are superimposed to reach receivers with different reception qualities [34]. However, in PxQAMA, the superposition of shared and private symbols occurs over the air, resulting in each user observing a distinct constellation. In contrast, the layered structure in LDM is formed at the transmitter, where all users receive an identical constellation consisting of the same core and extended layers.

C. Simple Receiver Processing

Based on (15), each user demodulates the bits contained in symbol \tilde{s}_u from the received signal y_u . Since different receivers follow the same steps, we drop the user index and simplify (15) as

$$y = e^{j\Phi} G \tilde{s} + w, \quad (21)$$

where $e^{j\Phi} G$ is the equivalent complex channel gain and should be determined before the receiver processing.

Regardless of how bit streams are layered and assigned, the receiver process of each user is as simple as the single-user receiver in an OMA system with a uniform QAM constellation. With more details available in [25], we summarize the main steps as follows.

- **Step 1:** One-tap equalization and I/Q decoupling are first performed on the received signal.

$$\tilde{y}^i := \Re\left\{\frac{e^{-j\Phi} y}{G}\right\} = \tilde{s}^i + \tilde{w}^i, \quad (22)$$

$$\tilde{y}^q := \Im\left\{\frac{e^{-j\Phi} y}{G}\right\} = \tilde{s}^q + \tilde{w}^q, \quad (23)$$

where \tilde{w}^i and \tilde{w}^q are the resulting noises.

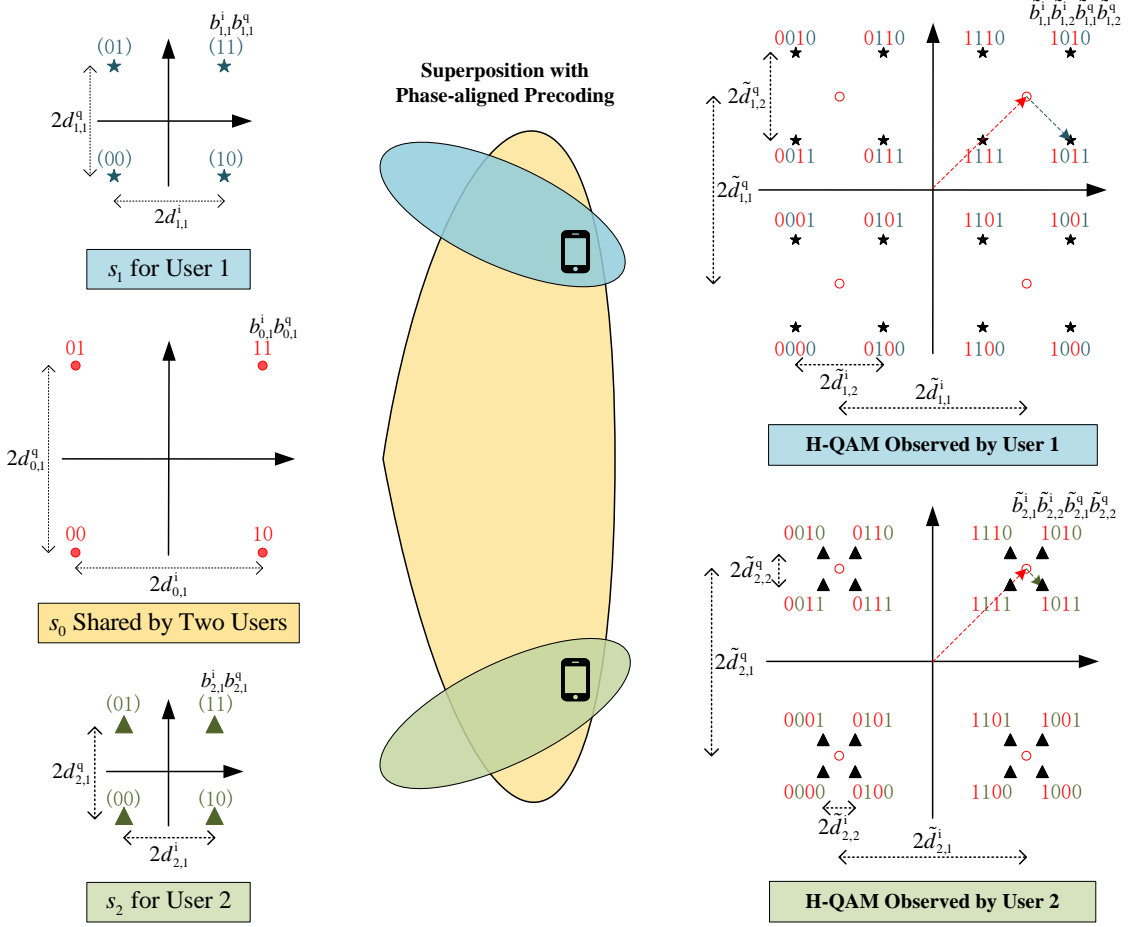


Fig. 3. Illustration of the system design with s_0, s_1, s_2 drawn from QPSK symbols, i.e., $m_i = n_i = 1, \forall i$. Two receivers observe Gray-coded H-16QAM constellations with different distance parameters.

- **Step 2:** Based on the distance parameters of the received constellation, each receiver calculates the log-likelihood ratio (LLR) of its own assigned bits. The real and imaginary components are processed separately in the same way. Taking the I branch as an example, the LLR for the κ -th bit \tilde{b}_κ^i is defined as

$$\Lambda(\tilde{b}_\kappa^i) = \ln \frac{f(\tilde{y}^i | \tilde{b}_\kappa^i = 1)}{f(\tilde{y}^i | \tilde{b}_\kappa^i = 0)}, \quad (24)$$

where $f(\tilde{y}^i | \tilde{b}_\kappa^i)$ denotes the likelihood function of the measurement \tilde{y}^i given \tilde{b}_κ^i . With the following definition

$$z_\kappa^i = \min_{\tilde{s} \in \mathcal{S}(\tilde{b}_\kappa^i = 0)} \frac{1}{4} |\tilde{y}^i - \tilde{s}|^2 - \min_{\tilde{s} \in \mathcal{S}(\tilde{b}_\kappa^i = 1)} \frac{1}{4} |\tilde{y}^i - \tilde{s}|^2, \quad (25)$$

the bit LLR is approximately by [25]:

$$\Lambda(\tilde{b}_\kappa^i) \approx \frac{4|G|^2}{\sigma^2} z_\kappa^i. \quad (26)$$

Note that a piecewise linear mapping operation can replace the dual-min operation in (25) for further complexity reduction [25]. Taking the I branch of H-64QAM

as an example, i.e., a hierarchical 8-PAM constellation, the approximated bit LLRs can be obtained as [25]

$$z_1^i = \begin{cases} \tilde{y}^i(\tilde{d}_1^i - \tilde{d}_2^i - \tilde{d}_3^i), & |\tilde{y}^i| \in [0, \tilde{d}_1^i - \tilde{d}_2^i) \\ (\tilde{d}_1^i - \tilde{d}_2^i)(\tilde{y}^i - \text{sign}(\tilde{y}^i)\tilde{d}_3^i), & |\tilde{y}^i| \in [\tilde{d}_1^i - \tilde{d}_2^i, \tilde{d}_1^i) \\ (\tilde{d}_1^i - \tilde{d}_3^i)(\tilde{y}^i - \text{sign}(\tilde{y}^i)\tilde{d}_2^i), & |\tilde{y}^i| \in [\tilde{d}_1^i, \tilde{d}_1^i + \tilde{d}_2^i) \\ \tilde{d}_1^i(\tilde{y}^i - \text{sign}(\tilde{y}^i)(\tilde{d}_2^i + \tilde{d}_3^i)), & |\tilde{y}^i| \in [\tilde{d}_1^i + \tilde{d}_2^i, \infty) \end{cases} \quad (27)$$

$$z_2^i = \begin{cases} \tilde{d}_2^i(\tilde{d}_1^i - \tilde{d}_3^i - |\tilde{y}^i|), & |\tilde{y}^i| \in [0, \tilde{d}_1^i - \tilde{d}_2^i) \\ (\tilde{d}_2^i - \tilde{d}_3^i)(\tilde{d}_1^i - |\tilde{y}^i|), & |\tilde{y}^i| \in [\tilde{d}_1^i - \tilde{d}_2^i, \tilde{d}_1^i + \tilde{d}_2^i) \\ \tilde{d}_2^i(\tilde{d}_1^i + \tilde{d}_3^i - |\tilde{y}^i|), & |\tilde{y}^i| \in [\tilde{d}_1^i + \tilde{d}_2^i, \infty) \end{cases} \quad (28)$$

$$z_3^i = \tilde{d}_3^i(\tilde{d}_2^i - |\tilde{d}_1^i - |\tilde{y}^i||). \quad (29)$$

- **Step 3:** Each user forwards the LLRs of its assigned bits into a channel decoder to recover the original message.

No SIC is needed at the receiver. Further, we have the following remarks on complexity.

- Each receiver has the same complexity as that in an OMA system with uniform QAM of the same constellation size $2^{m_0+m_u} \cdot 2^{m_0+n_u}$. Indeed, the same LLR computations

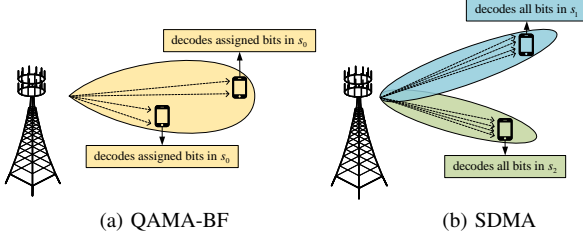


Fig. 4. The illustration of two special cases: (a) QAMA-BF and (b) SDMA, where the dashed lines represent the four bit streams considered in each beam.

can be used in both systems with the only difference on the values of the distance parameters.

- In all the simulation results, the constellation sizes for all receivers in PxQAMA are no larger than H-64QAM. Hence, the LLRs for three bits on the I branch and another three bits on the Q branch are computed based on the closed-form expressions in (27)-(29).

D. Two Special Cases

The general PxQAMA framework includes two important special cases as shown in Fig. 4.

- **QAMA with beamforming:** In this case, only one beam is formed with $\mathbf{x} = \mathbf{p}_0 s_0$, and the bits from two users are carried via the shared symbol s_0 , i.e., $m_1 = m_2 = n_1 = n_2 = 0$. Each user decodes the assigned bit streams in the received signal:

$$y_u = \mathbf{h}_u^H \mathbf{p}_0 s_0 + w_u. \quad (30)$$

This special case corresponds to the combination of QAMA with beamforming (QAMA-BF). Intuitively, this special configuration is useful when the channels from two users are highly correlated.

- **SDMA:** This configuration with no shared symbol, i.e., $m_0 = n_0 = 0$, is reduced to SDMA with $\mathbf{x} = \mathbf{p}_1 s_1 + \mathbf{p}_2 s_2$. With the directional control in (8), one obtains

$$y_u = \mathbf{h}_u^H \mathbf{p}_u s_u + w_u. \quad (31)$$

Intuitively, this special configuration is useful when the channels from two users are nearly orthogonal.

E. Extension to multi-user systems

We outline the extension of the PxQAMA framework to cases with $N_u > 2$ users. Similarly, coded bits from all users are split and mapped into one shared symbol s_0 and N_u private symbols $s_i, i \in \{1, \dots, N_u\}$. Bit streams from the shared symbol are assigned to different users and each private symbol is intended for a single user. Joint symbol mapping in (6) and (7) is adopted to ensure that the composite constellation of s_0 and s_i remains Gray-coded. Then the transmitted signal vector at each channel use becomes

$$\mathbf{x} = \mathbf{p}_0 s_0 + \sum_{i=1}^{N_u} \mathbf{p}_i s_i. \quad (32)$$

The directions of private symbol precoders are constrained as

$$\mathbf{h}_u^H \mathbf{p}_i = 0, \forall u \neq i. \quad (33)$$

Hence, \mathbf{p}_i is drawn from the null space of the channel vectors $\{\mathbf{h}_1, \dots, \mathbf{h}_{i-1}, \mathbf{h}_{i+1}, \dots, \mathbf{h}_{N_u}\}$. The phase alignment constraint for private symbol precoders becomes

$$e^{j\angle(\mathbf{h}_i^H \mathbf{p}_i)} = e^{j\angle(\mathbf{h}_i^H \mathbf{p}_0)} = e^{j\Phi_i}, \forall i. \quad (34)$$

As a result, the parallax effect remains in the multi-user cases, where each user observes a Gray-coded H-QAM constellation with individual distance parameters.

F. PxQAMA vs. One-layer RSMA

Although sharing the same expression for the transmitted vector in (2), PxQAMA and one-layer RSMA [11] are distinct from each other.

- The “message splitter” in RSMA is done on the information bits before channel coding. For a two-user system, there are three channel encoders at the transmitter side, one for the common stream, and one for each user’s private stream. Each receiver deploys two channel decoders, one for the common stream, and one for its own private stream. In total, there are three encoders at the transmitter and four decoders at the receivers for a two-user one-layer RSMA system. The split and joint modulation in PxQAMA is done on the bits after channel coding. There are two encoders and two decoders in the PxQAMA system.
- In RSMA, the common stream needs to be decoded successfully by all users. As a result, the data rate of the common stream is limited by the user with the worst channel quality. In PxQAMA, the shared symbol carries bit streams assigned to different users. Hence each receiver only demodulates its own bits, without any operation on the bits from the other user.
- RSMA can adopt SIC-free receivers to avoid the drawbacks of SIC receivers [30]. However, the complexity of the SIC-free receivers are still higher than the simple receivers for PxQAMA. This is because each user in the PxQAMA system observes a hierarchical QAM constellation with Gray mapping, which can be efficiently processed at the I and Q branches with simple LLR computation. RSMA adopts conventional constellations for the common and private data streams and the composite constellation at each receiver does not have a well-defined structure with Gray-mapping.

III. SYSTEM OPTIMIZATION

In this section, our objective is to determine the achievable rate region of the proposed system. To that end, we determine the closed-form solution to the precoder direction and phase shift, followed by the information rate calculation and the optimization framework for the proposed system.

A. Precoder Design

For convenience, we separate the norm of a vector from its direction by introducing unit-norm vectors as

$$\begin{cases} \mathbf{h}_u = |\mathbf{h}_u| \tilde{\mathbf{h}}_u = \lambda_u \tilde{\mathbf{h}}_u, & u = 1, 2, \\ \mathbf{p}_i = |\mathbf{p}_i| \tilde{\mathbf{p}}_i = \alpha_i \tilde{\mathbf{p}}_i, & i = 0, 1, 2, \end{cases} \quad (35)$$

where the vectors marked with tilde have unit norms. The variables λ_u and α_i respectively denote the norm of the channel and the norm of the precoding vector, respectively. Define the complex correlation coefficient ρ as

$$\rho = |\rho| e^{j\angle\rho} = \tilde{\mathbf{h}}_1^H \tilde{\mathbf{h}}_2, \quad (36)$$

where $\angle\rho \in [-\pi, \pi]$ is called the vectors' pseudo-angle [35]. Moreover, the Hermitian angle Θ between the normalized channel vectors $\tilde{\mathbf{h}}_1$ and $\tilde{\mathbf{h}}_2$ is defined as [36]

$$\Theta = \arccos(|\rho|), \quad (37)$$

and the chordal distance between $\tilde{\mathbf{h}}_1$ and $\tilde{\mathbf{h}}_2$ is [36]

$$\sin(\Theta) = \sqrt{1 - |\rho|^2}. \quad (38)$$

Through the Gram-Schmidt orthogonalization process, one can find two basic directions that cover the space spanned by $[\mathbf{h}_1, \mathbf{h}_2]$ as

$$\begin{cases} \tilde{\mathbf{q}}_1 = \tilde{\mathbf{h}}_1, \\ \tilde{\mathbf{q}}_2 = \frac{\tilde{\mathbf{h}}_2 - \rho \tilde{\mathbf{h}}_1}{\sqrt{1 - |\rho|^2}}. \end{cases} \quad (39)$$

1) Key Parameter for Shared Symbol Precoder Direction:

For the shared symbol, the optimal precoding vector $\tilde{\mathbf{p}}_0$ shall be placed in the range space of $\tilde{\mathbf{h}}_1$ and $\tilde{\mathbf{h}}_2$. Otherwise, energy is lost without benefiting any user. We can hence set the precoding direction of the shared symbol as a linear combination of $\tilde{\mathbf{q}}_1$ and $\tilde{\mathbf{q}}_2$ as

$$\tilde{\mathbf{p}}_0 = [\tilde{\mathbf{q}}_1, \tilde{\mathbf{q}}_2] \begin{bmatrix} \cos(\theta_0) \\ e^{j\phi_0} \sin(\theta_0) \end{bmatrix}, \quad (40)$$

where ϕ_0 and θ_0 are tunable parameters. By combining (39) and (40), one can verify that

$$\begin{cases} |\tilde{\mathbf{h}}_1^H \tilde{\mathbf{p}}_0| = \cos(\theta_0), \\ |\tilde{\mathbf{h}}_2^H \tilde{\mathbf{p}}_0| = |\rho^* \cos(\theta_0) + \sqrt{1 - |\rho|^2} \sin(\theta_0) e^{j\phi_0}|, \end{cases} \quad (41)$$

To maximize the right side of the second equation in (41), the two complex terms that are added together must have aligned phases. So we can first determine the optimal $\phi_0 = -\angle\rho$. Then with (37), we can verify that $|\tilde{\mathbf{h}}_2^H \tilde{\mathbf{p}}_0|$ reaches its maximum value of $|\cos(\Theta - \theta_0)|$. Hence, we express the optimized beam direction corresponding to the shared symbol as

$$\begin{aligned} \tilde{\mathbf{p}}_0 &= \cos(\theta_0) \tilde{\mathbf{q}}_1 + e^{-j\angle\rho} \sin(\theta_0) \tilde{\mathbf{q}}_2 \\ &= \frac{\sin(\Theta - \theta_0)}{\sin(\Theta)} \tilde{\mathbf{h}}_1 + \frac{\sin(\theta_0)}{\sin(\Theta)} e^{-j\angle\rho} \tilde{\mathbf{h}}_2, \end{aligned} \quad (42)$$

which has only one tunable parameter θ_0 . Substituting (42) into (41), we have

$$\begin{cases} \tilde{\mathbf{h}}_1^H \tilde{\mathbf{p}}_0 = \cos(\theta_0), \\ \tilde{\mathbf{h}}_2^H \tilde{\mathbf{p}}_0 = \cos(\Theta - \theta_0) e^{-j\angle\rho}. \end{cases} \quad (43)$$

It reveals that the beam direction determined by θ_0 is a trade-off between two users' equivalent channel gains of the shared symbol.

2) Closed-Form Solution to Private Symbol Precoders:

Given the shared symbol precoder $\tilde{\mathbf{p}}_0$ in (42), we further determine the precoding vector for two private symbols, whose direction and phase shift are constrained by (8) and (9).

Choosing the directions in the range space of $\tilde{\mathbf{h}}_1$ and $\tilde{\mathbf{h}}_2$, we can explicitly express the directions satisfying the orthogonality constraint as

$$\begin{cases} \tilde{\mathbf{p}}_1 = \frac{e^{j\phi_1}}{\sqrt{1 - |\rho|^2}} (\tilde{\mathbf{h}}_1 - \rho^* \tilde{\mathbf{h}}_2), \\ \tilde{\mathbf{p}}_2 = \frac{e^{j\phi_2}}{\sqrt{1 - |\rho|^2}} (\tilde{\mathbf{h}}_2 - \rho \tilde{\mathbf{h}}_1), \end{cases} \quad (44)$$

where ϕ_1 and ϕ_2 are tunable phase parameters for $\tilde{\mathbf{p}}_1$ and $\tilde{\mathbf{p}}_2$. Hence we have $\angle(\tilde{\mathbf{h}}_1^H \tilde{\mathbf{p}}_1) = \phi_1, \angle(\tilde{\mathbf{h}}_2^H \tilde{\mathbf{p}}_2) = \phi_2$. The phase alignment constraint in (9) could be satisfied by setting $\phi_1 = 0, \phi_2 = -\angle\rho$. Hence we have the closed-form solution to the extended symbol precoder direction as

$$\begin{cases} \tilde{\mathbf{p}}_1 = \frac{1}{\sqrt{1 - |\rho|^2}} (\tilde{\mathbf{h}}_1 - \rho^* \tilde{\mathbf{h}}_2), \\ \tilde{\mathbf{p}}_2 = \frac{e^{-j\angle\rho}}{\sqrt{1 - |\rho|^2}} (\tilde{\mathbf{h}}_2 - \rho \tilde{\mathbf{h}}_1). \end{cases} \quad (45)$$

To summarize, we decompose the precoder design into power and direction components, focusing on the latter in this subsection. The shared symbol precoder direction is controlled by θ_0 , which balances the equivalent channel gains of the two users. For the private symbol, the precoding vectors have a closed-form solution as in (45) due to the orthogonality and phase alignment constraints.

B. Information Rates for the Bit Streams

Substituting precoder designs in (42) and (45) into the received signal model in (15), we have

$$\begin{aligned} y_1 &= G_1 \tilde{s}_1 + w_1, \\ y_2 &= e^{-j\angle\rho} G_2 \tilde{s}_2 + w_2. \end{aligned} \quad (46)$$

where the modulus of equivalent channel gains are

$$\begin{aligned} G_1 &= \sqrt{[\lambda_1 \alpha_0 \cos(\theta_0)]^2 + [\lambda_1 \alpha_1 \sin(\Theta)]^2} \\ G_2 &= \sqrt{[\lambda_2 \alpha_0 \cos(\Theta - \theta_0)]^2 + [\lambda_2 \alpha_2 \sin(\Theta)]^2} \end{aligned} \quad (47)$$

The distance parameters in (18) and (19) for the constellations of \tilde{s}_1 and \tilde{s}_2 on the I branch can be simplified to

$$\begin{aligned} \tilde{d}_{1,\kappa}^i &= \begin{cases} \frac{\lambda_1 \alpha_0 \cos(\theta_0)}{G_1} d_{0,\kappa}^i & \text{if } \kappa \leq m_0, \\ \frac{\lambda_1 \alpha_1 \sin(\Theta)}{G_1} d_{1,\kappa-m_0}^i & \text{if } \kappa > m_0, \end{cases} \\ \tilde{d}_{2,\kappa}^i &= \begin{cases} \frac{\lambda_2 \alpha_0 \cos(\Theta - \theta_0)}{G_2} d_{0,\kappa}^i & \text{if } \kappa \leq m_0, \\ \frac{\lambda_2 \alpha_2 \sin(\Theta)}{G_2} d_{2,\kappa-m_0}^i & \text{if } \kappa > m_0, \end{cases} \end{aligned} \quad (48)$$

The expressions on the Q branch are similar and hence omitted for brevity.

Based on the equivalent channel and the known distance parameters for the constellation, the information rate of bit streams can be determined. Specifically, based on the received

symbol y_u , the LLRs for the bits in \tilde{s}_u , i.e., $\{\tilde{b}_{u,\kappa}^i, \tilde{b}_{u,l}^q\}$ are generated as $\{z_{u,\kappa}^i, z_{u,l}^q\}$. The mutual information between each bit and the LLR can be found via the reduction of the uncertainty when conditioned on the bit value, as detailed in [25]. For user u , we can determine all the relevant mutual information as

$$\left\{ I(\tilde{b}_{u,\kappa}^i) \right\}_{\kappa=1}^{m_0+m_u}, \left\{ I(\tilde{b}_{u,l}^q) \right\}_{l=1}^{n_0+n_u}. \quad (49)$$

C. Rate Region of PxQAMA

We now determine the achievable rate region of the proposed system. The following parameters are adjustable to provide different rates for different users.

- **Bit-to-user Assignment:** The bits from \mathcal{S}_0 can be assigned to different users:

$$\mathcal{S}_0 = \mathcal{S}_{0,1} \cup \mathcal{S}_{0,2}, \quad (50)$$

where $\mathcal{S}_{0,u}$ denotes the collection of bits assigned to user u in \mathcal{S}_0 . Let \mathcal{A}_u denote the collection of all bits assigned to user u . Under the PxQAMA framework, we have

$$\mathcal{A}_1 = \mathcal{S}_{0,1} \cup \mathcal{S}_1, \quad \mathcal{A}_2 = \mathcal{S}_{0,2} \cup \mathcal{S}_2. \quad (51)$$

Each receiver u can identify its own bits from \tilde{s}_u based on \mathcal{A}_u and the relationship in (16) and (17). Based on the mutual information in (49), the achievable rate of user u is

$$R_u = \sum_{\tilde{b}_{u,\kappa}^i \in \mathcal{A}_u} I(\tilde{b}_{u,\kappa}^i) + \sum_{\tilde{b}_{u,l}^q \in \mathcal{A}_u} I(\tilde{b}_{u,l}^q). \quad (52)$$

- **Constellation Optimization:** As shown in [25], optimized H-QAM constellation is better than uniform QAM constellation. Hence the proposed transmitter needs to optimize the distances in $\mathcal{D}_0, \mathcal{D}_1, \mathcal{D}_2$ to expand the rate region.
- **Beam Direction Optimization and Power Allocation:** Optimization of beamforming vectors $\{\mathbf{p}_0, \mathbf{p}_1, \mathbf{p}_2\}$ can be decomposed into the optimization of each beam's power and direction. The beam direction of \mathbf{p}_0 can be adjusted by varying θ_0 in the range of $[0, \Theta]$. The power of each beam is adjusted by varying $\{\alpha_0, \alpha_1, \alpha_2\}$ under the constraint $\alpha_0^2 + \alpha_1^2 + \alpha_2^2 = 1$.

To summarize, the bit-to-user assignment, the distance parameters of the constellations, and the precoding vectors all affect the user rates. The proposed system first dynamically selects suitable modes for constellation sizes and bit assignments according to user deployments. For the given constellation size and bit assignment, equation (46) shows that the beam direction-related parameter θ_0 and power-related parameters $\alpha_0, \alpha_1, \alpha_2$ jointly control the equivalent channel gains of shared and private symbols for two users. By jointly varying $\theta_0, \alpha_0, \alpha_1, \alpha_2$ and distance parameters in $\mathcal{D}_0, \mathcal{D}_1, \mathcal{D}_2$, H-QAM constellations with different received distance parameters $\{\tilde{d}_{u,\kappa}^i, \tilde{d}_{u,l}^q\}$ are observed by each user. Hence, various rate points (R_1, R_2) are achieved by jointly adjusting the parameters mentioned above. Finally, the achievable rate region is determined as the *convex hull* of all rate points from individual parameter configurations.

IV. NUMERICAL RESULTS

In this section, we compare the achievable rate region of different access schemes in the two-user case with some specific channel realizations. We set $N_t = 2$ and consider channel vectors as

$$\mathbf{h}_1^H = \lambda_1[1, 0], \quad \mathbf{h}_2^H = \lambda_2[\rho, \sqrt{1-|\rho|^2}], \quad (53)$$

where λ_1, λ_2 and ρ control the channel strengths and the channel correlation between two users, respectively. As a result, the reference SNR of user k is defined as

$$\gamma_u = \frac{\lambda_u^2}{\sigma^2}. \quad (54)$$

All schemes in comparisons are summarized as follows.

- **DPC with Gaussian inputs (DPC-Gaussian):** Based on the algorithm in [37], we determine the capacity region achieved by DPC with Gaussian inputs.
- **PxQAMA:** Following steps described in section III-C, we determine the achievable rate region of the proposed scheme. Corresponding to the simple receiver processing, the data rates of bit-interleaved coded modulation (BICM) with H-QAM are evaluated. To simplify the search, the following constraints are imposed in PxQAMA systems:
 - Each branch of s_0, s_1, s_2 adopts a uniform PAM constellation, i.e., $\tilde{d}_{i,\kappa}^i = 2d_{i,\kappa+1}^i, \tilde{d}_{i,l}^q = 2d_{i,l+1}^q$.
 - s_1 and s_2 are drawn from constellations with the same size, i.e., $m_1 = m_2, n_1 = n_2$, although the corresponding distance parameters may differ.
- **1-Layer RSMA:** As a promising multiple access technique, the 1-Layer RSMA design with both SIC-based and non-SIC receivers are compared, denoted as RSMA-SIC and RSMA-NSIC, respectively. Then the constellation-constrained (CC) rates of RSMA systems with uniform QAM are evaluated based on the derivation described in [30], where nonbinary coded modulation (CM), achieving performance gain with the cost of receiver complexity, is involved. Note that zero-forcing (ZF) precoding is adopted for private streams, while the direction of the precoder for the common stream and the power allocated to each stream are exhaustively searched to determine the region.
- **SDMA:** As a special case of the proposed scheme with $m_0 = n_0 = 0$, SDMA is considered as a benchmark scheme. The data rates of BICM are evaluated.
- **NOMA:** By entirely encoding the message for the user with worse channel conditions into the common stream and turning off its private stream in RSMA systems, the rate region of NOMA is obtained. SIC-based receivers and nonbinary coded modulation are assumed as in RSMA-SIC.

Among all schemes in comparison, PxQAMA offers the lowest receiver complexity, benefiting from the elimination of SIC and the independent bit-wise demodulation process. In the simulations, the received constellation for all the users is no larger than H-64QAM. To this end, the combinations of different constellation sizes for each symbol are considered in all schemes. Then the rate region is determined as the convex

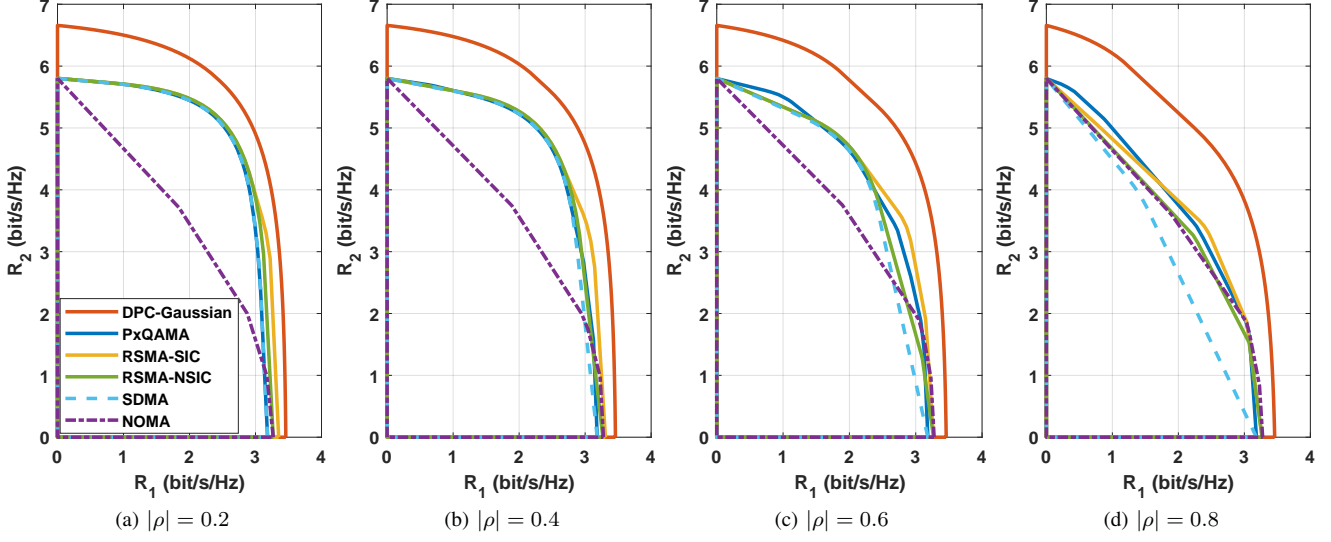


Fig. 5. Comparison of the rate region with $(\gamma_1, \gamma_2) = (10, 20)$ dB.

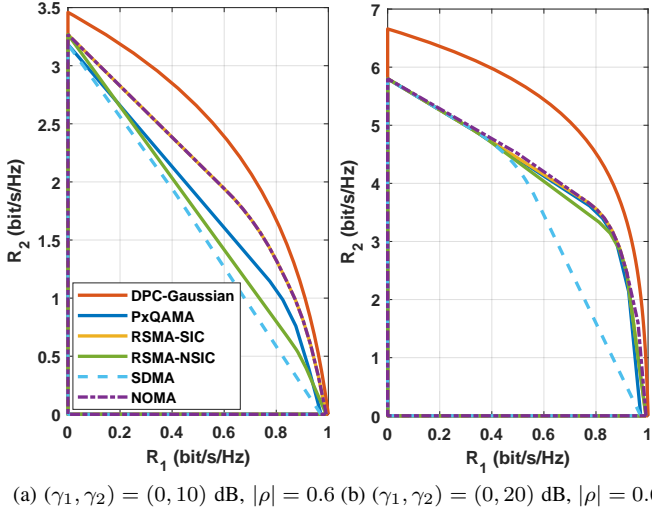


Fig. 6. Rate region comparison of different schemes with lower reference SNRs or larger channel strength difference.

hull of all rate points from individual combinations by the Matlab function `convhull()`.

A. Comparison of Rate Regions

Fig. 5 compares the achievable rate regions of the proposed system with all benchmark schemes, where reference SNRs at two users are set as $(\gamma_1, \gamma_2) = (10, 20)$ dB and various channel correlation are considered. Key observations are summarized as follows:

- Fig. 5(a) and Fig. 5(b) show that the rate region of all schemes except NOMA almost completely overlaps when user channels are sufficiently orthogonal (low $|\rho|$), as all schemes can reduce to SDMA, which performs well in these cases². Note that there are some rate gaps

²Hence the cases with relatively small $|\rho|$ are omitted in the following simulation results, and only the comparisons when $|\rho|$ is moderately high are presented to save space.

between corner points of different schemes, as CM rates are evaluated for RSMA and NOMA systems and BICM rates are evaluated for PxQAMA and SDMA systems.

- As shown in Fig. 5(c) and Fig. 5(d), the performance of SDMA degrades when the channel correlation increases. In contrast, NOMA achieves a good performance when user channels are sufficiently aligned (large $|\rho|$). Moreover, both PxQAMA and RSMA perform consistently well in various scenarios by dynamically adjusting the system configuration.
- We further compare the rate region of the PxQAMA and RSMA systems. When $|\rho|$ is relatively large, the performance of RSMA systems degrades due to the use of non-SIC receivers instead of SIC receivers. However, PxQAMA outperforms RSMA-NSIC despite adopting a simpler receiver. Moreover, PxQAMA achieves 97.8% and 100% of the rate region area of RSMA-SIC when $|\rho| = 0.6$ and $|\rho| = 0.8$, respectively, demonstrating its effectiveness in achieving near-optimal performance even without SIC. Note that the rate region of PxQAMA extends beyond that of RSMA-SIC in certain areas. This is because, in PxQAMA, the rate associated with the shared symbols is not subject to the worse channel condition of the two users. By comparison, in RSMA-SIC, the common stream's rate is constrained by such conditions.

Then we further investigate the impacts of relatively lower reference SNRs and larger channel strength differences on the rate region. Fig. 6(a) presents a comparison of rate regions of different schemes with $(\gamma_1, \gamma_2) = (0, 10)$ dB and $|\rho| = 0.6$. Compared with Fig. 5(c), when reference SNR decreases, the methods without SIC experience a greater rate loss than NOMA and RSMA-SIC do, despite the same channel strength differences. It reveals that, for low SNRs, decoding interference by SIC receivers becomes more efficient than suppressing interference in the spatial domain. Meanwhile, among the methods with non-SIC receivers, PxQAMA still demonstrates

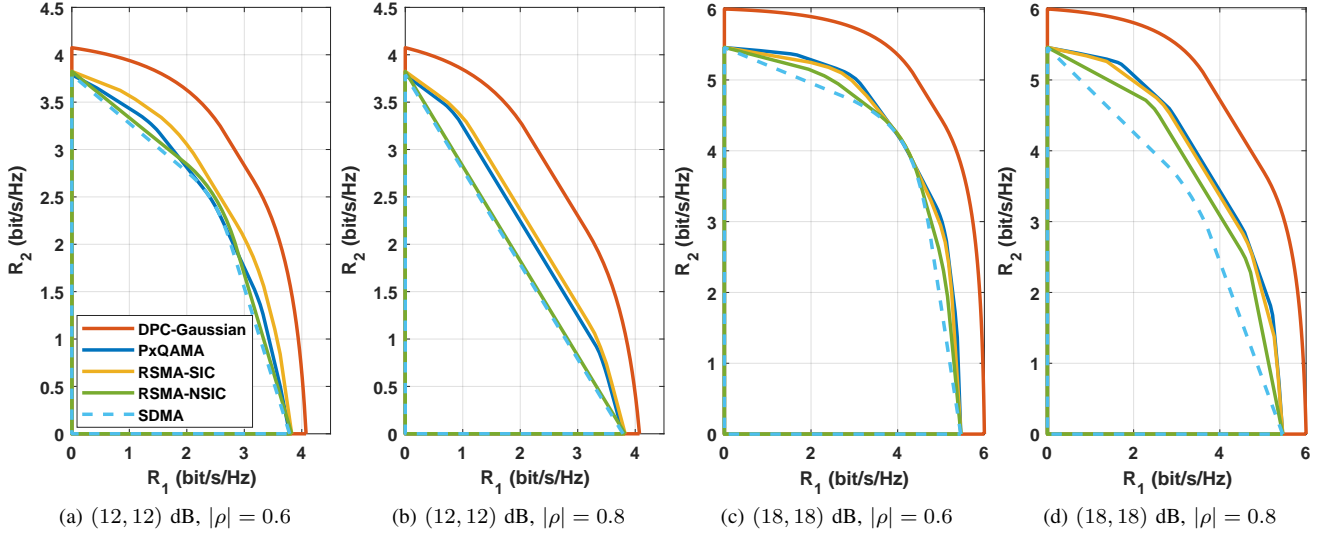


Fig. 7. Rate region comparison of different schemes with equal channel strengths ($\gamma_1 = \gamma_2$).

a superior performance over RSMA-NSIC and SDMA due to the well-designed structure of the received composite constellation with Gray-mapping. Specifically, for $R_1 = 0.8$ bps/Hz, PxQAMA demonstrates performance gains of 82% and 33% for user 2 relative to SDMA and RSMA-NSIC, respectively. Fig. 6(b) considers a larger channel strength difference with $(\gamma_1, \gamma_2) = (0, 20)$ dB and $|\rho| = 0.6$. Benefiting from the growth of channel strength differences, PxQAMA, along with RSMA-SIC, RSMA-NSIC and NOMA, achieves a larger rate region than SDMA in this case. Specifically, when $R_1 = 0.8$ bps/Hz, all other methods achieve a significant gain of around 119% for user 2 over SDMA. Meanwhile, both PxQAMA and RSMA-NSIC achieve similar rate regions as the schemes with SIC-based receivers because interference and signal are more distinguishable due to significant power differences in such cases.

We further compare the rate regions of different schemes under equal channel strength conditions, i.e., $\gamma_1 = \gamma_2$. The rate region of NOMA is omitted as it performs inefficiently when there is no channel strength disparity. As shown in Fig. 7, both PxQAMA and RSMA-SIC outperform SDMA due to the flexible system framework. Meanwhile, performance loss of RSMA caused by the absence of SIC receivers is observed in all sub-figures. Compared to RSMA-NSIC, the proposed PxQAMA system achieves a larger rate region with a simpler receiver. Even compared to RSMA systems with SIC receivers, PxQAMA achieves almost the same rate region as shown in Fig. 7(b)–(d).

B. Selection of Transmission Modes

The achievable rate region of PxQAMA is determined by the convex hull of many discrete rate points. Each rate point corresponds to the achieved (R_1, R_2) corresponding to one transmitter configuration of the H-QAM constellations, the bit-to-user assignment, and the power splitting among the shared and private symbols. Each configuration is termed as a *transmission mode*.

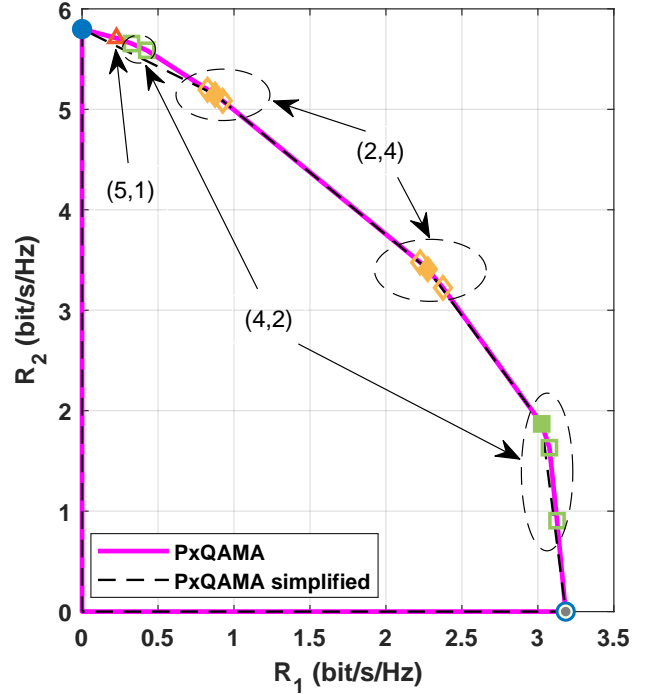


Fig. 8. The two-user rate region with $(\gamma_1, \gamma_2) = (10, 20)$ dB and $|\rho| = 0.8$ is formed by 14 discrete rate points in a few separated clusters, where each point corresponds to a specific configuration for $(m_0 + n_0, m_1 + n_1)$. A polygon formed by five selected transmission modes, each labeled by a filled marker, approximates the rate region.

For the setting in Fig. 8, a total of $N_1 = 14$ rate points are marked on the Pareto-frontier of the rate curve. In practice, one can reduce the number of transmission modes following a procedure outlined in [25]. Fig. 8 provides a demonstration with the original rate region approximated by a polygon formed by $N_2 = 5$ selected transmission modes: two modes of OMA, two modes with $(m_0 + n_0, m_1 + n_1) = (2, 4)$, and one mode with $(m_0 + n_0, m_1 + n_1) = (4, 2)$. Note that m_2, n_2 are omitted due to the assumption $m_1 = m_2, n_1 = n_2$. The loss of

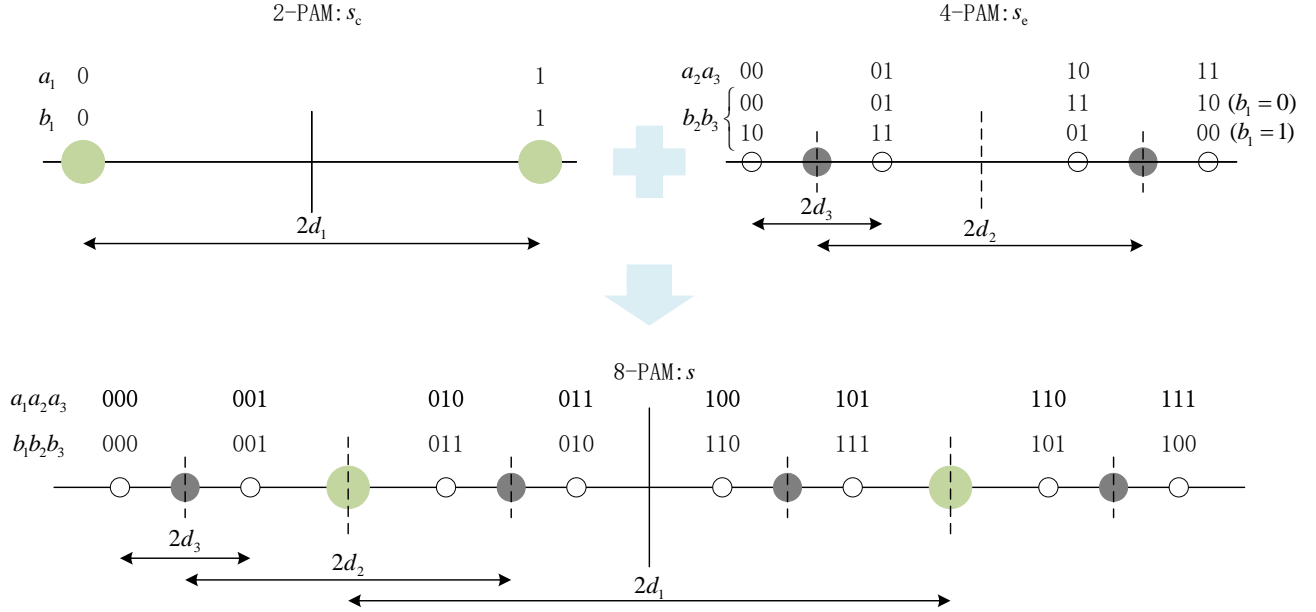


Fig. 9. The hierarchical 2-PAM and 4-PAM constellation could linearly add up to a composite Gray-coded 8-PAM by joint modulation, where the mapping rule for the high-layer constellation is dependent on the bits in the low-layer constellation.

the area formed by the polygon with five transmission modes relative to the original rate region is negligible. An upper-layer scheduler can utilize these transmission modes to achieve a rate pair on any point of the polygon via time sharing, while always maintaining low complexity at the receivers.

V. CONCLUSION

In this paper, we presented a downlink multiple access scheme based on joint symbol mapping of H-QAM constellations and phase-aligned precoding. Benefiting from the ingenious designs at the transmitter, a unique parallax effect appears in the proposed PxQAMA system, where each receiver observes an individual Gray-coded H-QAM constellation shaped by the user channel. Large rate region is achieved by PxQAMA while the receiver complexity remains as low as that in an OMA system. Hence PxQAMA shows great potential for future 6G and IoT systems, where both receiver complexity and achievable rate are critical metrics. The extension of the proposed scheme to the multi-user broadband system and the optimization with imperfect channel state information are interesting directions for future research.

APPENDIX

HIERARCHICAL QAM WITH GRAY MAPPING

Consider a real hierarchical M -ary PAM constellation with distance parameters $\{d_1, \dots, d_m\}$, where $m = \log_2 M$. There are a total of M constellation points located at $\{\pm d_1 \pm d_2 \dots \pm d_m\}$ on the real line, satisfying $d_k \geq 2d_{k+1}$ for $k = 1, \dots, m-1$. Index these points with 0 to $M-1$ from left to right. For a constellation point, denote the bits of natural mapping and the Gray mapping as

$$\begin{cases} \text{Natural mapping:} & [a_1, \dots, a_m] \\ \text{Gray mapping:} & [b_1, \dots, b_m] \end{cases} \quad (55)$$

The natural mapping $\{a_1, \dots, a_m\}$ is obtained from the binary representation of the index of the constellation point. Eq. (9) from [32] specifies that the constellation point can be computed from the bits from natural mapping as

$$s = \sum_{\kappa=1}^m (2a_{\kappa} - 1)d_{\kappa}. \quad (56)$$

Equation (1) from [32] specifies how to obtain the bits of Gray mapping b_m from the bits of natural mapping via

$$\begin{aligned} b_1 &= a_1, \\ b_{\kappa} &= a_{\kappa} \oplus a_{\kappa-1}, \kappa = 2, \dots, m, \end{aligned} \quad (57)$$

where \oplus represents modulo-2 addition.

Combining (56) and (57), one can identify the constellation point via the bits of Gray mapping directly. First, we revert the Gray encoding in (57) as

$$a_{\kappa} = b_{\kappa} \oplus b_{\kappa-1} \dots \oplus b_1. \quad (58)$$

Second, we rewrite (56) as

$$s = \sum_{\kappa=1}^m (-1)^{1+\sum_{j=1}^{\kappa} b_j} d_{\kappa}. \quad (59)$$

Combining (58) and (59), we obtain:

$$s = \sum_{\kappa=1}^m (-1)^{(1+\sum_{j=1}^{\kappa} b_j)} d_{\kappa}. \quad (60)$$

The key insight based on the expression in (60) is that the symbol s can be decomposed to two symbols as

$$s = \underbrace{\sum_{\kappa=1}^{m_0} (-1)^{(1+\sum_{j=1}^{\kappa} b_j)} d_{\kappa}}_{s_c} + \underbrace{(-1)^{(1+\sum_{j=1}^{m_0} b_j)} \sum_{\kappa=m_0+1}^m (-1)^{(\sum_{j=m_0+1}^{\kappa} b_j)} d_{\kappa}}_{s_e}. \quad (61)$$

With the terminology from hierarchical constellation, one can view s_c as a symbol at the core layer and s_e as a symbol at the extended layer [34].

Fig. 9 illustrates the linear superposition of 2-PAM and 4-PAM component constellations, forming a Gray-coded hierarchical 8-PAM composite constellation. The key is that the mapping rule for s_e on the extended layer is dependent on the value of bits for s_c on the core layer.

For H-QAM constellation, Gray coding is applied separately on the PAM constellations on the I and Q branches.

REFERENCES

- [1] E. A. Jorswieck, "Next-generation multiple access: From basic principles to modern architectures," *Proceedings of the IEEE*, vol. 112, no. 9, pp. 1149–1178, 2024.
- [2] T. Cover, "Broadcast channels," *IEEE Transactions on Information Theory*, vol. 18, no. 1, pp. 2–14, 1972.
- [3] D. Tse, *Fundamentals of Wireless Communication*. Cambridge University Press, 2005.
- [4] H. Weingarten, Y. Steinberg, and S. S. Shamai, "The capacity region of the Gaussian multiple-input multiple-output broadcast channel," *IEEE transactions on information theory*, vol. 52, no. 9, pp. 3936–3964, 2006.
- [5] A. Goldsmith, S. Jafar, N. Jindal, and S. Vishwanath, "Capacity limits of MIMO channels," *IEEE Journal on Selected Areas in Communications*, vol. 21, no. 5, pp. 684–702, 2003.
- [6] T. Yoo and A. Goldsmith, "On the optimality of multiantenna broadcast scheduling using zero-forcing beamforming," *IEEE Journal on selected areas in communications*, vol. 24, no. 3, pp. 528–541, 2006.
- [7] B. Clerckx and C. Oestges, *MIMO wireless networks: channels, techniques and standards for multi-antenna, multi-user and multi-cell systems*. Academic Press, 2013.
- [8] L. Dai, B. Wang, Z. Ding, Z. Wang, S. Chen, and L. Hanzo, "A survey of non-orthogonal multiple access for 5G," *IEEE Communications Surveys & Tutorials*, vol. 20, no. 3, pp. 2294–2323, 2018.
- [9] Y. Liu, S. Zhang, X. Mu, Z. Ding, R. Schober, N. Al-Dhahir, E. Hossain, and X. Shen, "Evolution of NOMA toward next generation multiple access (NGMA) for 6G," *IEEE Journal on Selected Areas in Communications*, vol. 40, no. 4, pp. 1037–1071, 2022.
- [10] Z. Ding, F. Adachi, and H. V. Poor, "The application of MIMO to non-orthogonal multiple access," *IEEE Transactions on Wireless Communications*, vol. 15, no. 1, pp. 537–552, 2015.
- [11] Y. Mao, O. Dizdar, B. Clerckx, R. Schober, P. Popovski, and H. V. Poor, "Rate-splitting multiple access: Fundamentals, survey, and future research trends," *IEEE Communications Surveys & Tutorials*, 2022.
- [12] B. Clerckx, Y. Mao, R. Schober, and H. V. Poor, "Rate-splitting unifying SDMA, OMA, NOMA, and multicasting in MISO broadcast channel: A simple two-user rate analysis," *IEEE Wireless Communications Letters*, vol. 9, no. 3, pp. 349–353, 2019.
- [13] Y. Mao, B. Clerckx, and V. O. Li, "Rate-splitting multiple access for downlink communication systems: Bridging, generalizing, and outperforming SDMA and NOMA," *EURASIP journal on wireless communications and networking*, vol. 2018, pp. 1–54, 2018.
- [14] H. Joudeh and B. Clerckx, "Robust transmission in downlink multiuser MISO systems: A rate-splitting approach," *IEEE Transactions on Signal Processing*, vol. 64, no. 23, pp. 6227–6242, 2016.
- [15] M. Dai, B. Clerckx, D. Gesbert, and G. Caire, "A rate splitting strategy for massive MIMO with imperfect CSIT," *IEEE Transactions on Wireless Communications*, vol. 15, no. 7, pp. 4611–4624, 2016.
- [16] H. Joudeh and B. Clerckx, "Rate-splitting for max-min fair multigroup multicast beamforming in overloaded systems," *IEEE Transactions on Wireless Communications*, vol. 16, no. 11, pp. 7276–7289, 2017.
- [17] Y. Mao, B. Clerckx, and V. O. Li, "Energy efficiency of rate-splitting multiple access, and performance benefits over SDMA and NOMA," in *2018 15th International Symposium on Wireless Communication Systems (ISWCS)*, 2018, pp. 1–5.
- [18] E. Piovano and B. Clerckx, "Optimal DoF region of the K-user MISO BC with partial CSIT," *IEEE Communications Letters*, vol. 21, no. 11, pp. 2368–2371, 2017.
- [19] X. Lyu, S. Aditya, J. Kim, and B. Clerckx, "Rate-splitting multiple access: The first prototype and experimental validation of its superiority over SDMA and NOMA," *IEEE Transactions on Wireless Communications*, vol. 23, no. 8, pp. 9986–10000, 2024.
- [20] B. Clerckx, Y. Mao, R. Schober, E. A. Jorswieck, D. J. Love, J. Yuan, L. Hanzo, G. Y. Li, E. G. Larsson, and G. Caire, "Is NOMA efficient in multi-antenna networks? a critical look at next generation multiple access techniques," *IEEE Open Journal of the Communications Society*, vol. 2, pp. 1310–1343, 2021.
- [21] A. S. de Sena, F. R. M. Lima, D. B. da Costa, Z. Ding, P. H. J. Nardelli, U. S. Dias, and C. B. Papadias, "Massive MIMO-NOMA networks with imperfect SIC: Design and fairness enhancement," *IEEE Transactions on Wireless Communications*, vol. 19, no. 9, pp. 6100–6115, 2020.
- [22] S.-L. Shieh and Y.-C. Huang, "A simple scheme for realizing the promised gains of downlink nonorthogonal multiple access," *IEEE Transactions on Communications*, vol. 64, no. 4, pp. 1624–1635, 2016.
- [23] M. Qiu, Y.-C. Huang, S.-L. Shieh, and J. Yuan, "A lattice-partition framework of downlink non-orthogonal multiple access without SIC," *IEEE Transactions on Communications*, vol. 66, no. 6, pp. 2532–2546, 2018.
- [24] D. Fang, Y.-C. Huang, G. Geraci, Z. Ding, and H. Claussen, "Enhanced multiuser superposition transmission through structured modulation," *IEEE Transactions on Wireless Communications*, vol. 18, no. 5, pp. 2765–2776, 2019.
- [25] J. Zhu, S. Zhou, and M. Zhao, "QAMA: Hierarchical QAM based downlink multiple access with a simple receiver," *IEEE Transactions on Wireless Communications*, vol. 23, no. 10, pp. 12 565–12 577, 2024.
- [26] 3GPP TR 36.859 V13.0.0 (2015-12), "Technical Specification Group Radio Access Network; Study on Downlink Multiuser Superposition Transmission (MUST) for LTE (Release 13)," Dec 2015.
- [27] G. Arora and A. Jaiswal, "Zero SIC based rate splitting multiple access technique," *IEEE Communications Letters*, vol. 26, no. 10, pp. 2430–2434, 2022.
- [28] A. S. de Sena, P. H. J. Nardelli, D. B. da Costa, P. Popovski, C. B. Papadias, and M. Debbah, "Dual-polarized massive MIMO-RSMA networks: Tackling imperfect SIC," *IEEE Transactions on Wireless Communications*, vol. 22, no. 5, pp. 3194–3215, 2023.
- [29] S. Zhang, B. Clerckx, and D. Vargas, "SIC-free rate-splitting multiple access: Constellation constrained sum-rate optimization," in *2024 IEEE 25th International Workshop on Signal Processing Advances in Wireless Communications (SPAWC)*, 2024, pp. 903–910.
- [30] S. Zhang, B. Clerckx, D. Vargas, O. Haffenden, and A. Murphy, "Rate-splitting multiple access: Finite constellations, receiver design, and SIC-free implementation," *IEEE Transactions on Communications*, vol. 72, no. 9, pp. 5319–5333, 2024.
- [31] P. Vitthaladevuni and M.-S. Alouini, "A recursive algorithm for the exact BER computation of generalized hierarchical QAM constellations," *IEEE Transactions on Information Theory*, vol. 49, no. 1, pp. 297–307, 2003.
- [32] —, "A closed-form expression for the exact BER of generalized PAM and QAM constellations," *IEEE Transactions on Communications*, vol. 52, no. 5, pp. 698–700, 2004.
- [33] ATSC Standard: A/322, "Physical Layer Protocol, document A322," Advanced Television Systems Committee, Dec. 2018.
- [34] L. Zhang, W. Li, Y. Wu, X. Wang, S.-I. Park, H. M. Kim, J.-Y. Lee, P. Angueira, and J. Montalban, "Layered-division-multiplexing: Theory and practice," *IEEE Transactions on Broadcasting*, vol. 62, no. 1, pp. 216–232, 2016.
- [35] K. Scharnhorst, "Angles in complex vector spaces," *Acta Applicandae Mathematicae*, no. 69, p. 95–103, 2001.
- [36] J. H. Conway, R. H. Hardin, and N. J. A. Sloane, "Packing lines, planes, etc.: Packings in Grassmannian space," *Experimental Math.*, vol. 5, no. 2, pp. 139–159, 1996.
- [37] H. Viswanathan, S. Venkatesan, and H. Huang, "Downlink capacity evaluation of cellular networks with known-interference cancellation," *IEEE Journal on Selected Areas in Communications*, vol. 21, no. 5, pp. 802–811, 2003.